INTERNATIONAL JOURNAL OF CLIMATOLOGY
Int. J. Climatol. **35**: 69–84 (2015)
Published online 9 May 2014 in Wiley Online Library
(wileyonlinelibrary.com) DOI: 10.1002/joc.3963

Global distribution and risk to shipping of very extreme sea states (VESS)

V. J. Cardone,[a†] B. T. Callahan,[a] H. Chen,[b] A. T. Cox,[a*] M. A. Morrone[a] and V. R. Swail[c]

[a] *Oceanweather Inc., Cos Cob, CT, USA*
[b] *Jeppesen Marine, Almeda, CA, USA*
[c] *Environment Canada, Toronto, ON, Canada*

ABSTRACT: The impact of extreme sea states on offshore infrastructure is of intense interest in the ocean engineering community at the present time. In this study, a new quality-controlled database of global satellite-derived estimates of significant wave height (HS) and surface marine wind speed from seven missions spanning the period August 1991–March 2010, known as GlobWave, is scanned to yield over 5000 ocean basin specific orbit segments with peak HS > 12 m. This population was subsequently distilled to a population of 120 individual storms [so-called very extreme sea states (VESS) storms], in which there was at least one altimeter estimate of HS > 16 m. The highest HSs were observed in the Northern Hemisphere with ten orbit segments in the North Atlantic Ocean (NAO) with a peak HS of >18 m followed by four segments in the North Pacific Ocean (NPO). Only three HS peaks >18 m were seen in the entire Southern Oceans. Three of the >5000 orbit segments had a peak HS >20 m with the highest at 20.6 m. The number of VESS storms detected is greatest in the NAO (the smallest basin), a result that appears to be consistent with general circulation studies of extratropical cyclogenesis frequency and intensity in general atmospheric circulation models.

A new continuous 33-year global wave hindcast (GROW2012) based on a new atmospheric reanalysis wind field product appears to provide unbiased estimates of the probability of exceedance of VESS in extratropical storms and small-basin dependent biases (0.5–1.5 m) of peak HS greater than ~16 m. GROW2012 was, therefore, applied with a voyage simulator for nine trade routes to assess the risk of a merchant vessel that does not avail itself of weather routing of encountering VESS. The highest monthly exceedance probabilities (MEPs) at the VESS threshold of 14 m are found in the NAO and NPO at ~0.1% during winter months. The alternative statistical distribution of the MEP of the single maximum peak sea state to be expected for a voyage for any month (MEPm) shows that the highest MEPm is for the month of December in the NAO along the great circle route between the middle US East Coast and entrance to English Channel and in the NPO along the Yokohama–Seattle route, at about 3%. Still, the overall probability of a vessel encountering sea states that may contain waves capable of catastrophic damage over a 33-year lifetime is quite small with mean number of hours of exposure to a vessel typically less than ~3 h for six of the nine routes and a maximum of 10 h for two of the routes.

KEY WORDS shipping; waves; extremes; hindcasting

Received 21 June 2013; Revised 22 January 2014; Accepted 23 January 2014

1. Introduction

1.1. Sea state and vessel design

Sea state is a critical element of design of vessels and offshore structures, carrying out marine operations, tactical voyage planning and management and forensic investigations following accidents in heavy weather. As design processes have evolved, the requirements for greater detail in the specification of sea state design criteria have increased. The most basic sea state description for vessel design has been the wave height–wave period bivariate frequency of occurrence distribution often referred to as a 'scatter diagram' (e.g. International Association of Classification Societies (IACS) Rec. 34, see IACS, 2001) based on summarization of historical collections of visual observations of sea state from merchant vessels participating in the Voluntary Observations from Ships (VOS) program. Traditionally, the scatter diagram pertaining to open North Atlantic wave climate has been adopted for ship design. Following the landmark work of St. Denis and Pierson (1953) needs have expanded to a description of the full wave spectrum to allow the prediction of ship responses following a statistical approach. This requirement was first satisfied by the development of an analytical form for the frequency spectrum of fully developed seas based on measurements of shipborne wave recorders on weather ships deployed in the eastern North Atlantic Ocean (NAO) in the late 1950s (Pierson and Moskowitz, 1964). It is interesting to note that in their binning of measured weather ship spectral data to form average spectra, the most extreme average group for which a reliable statistical average could be formed by Pierson and Moskowitz was associated with a wind speed of ~20 m s^{-1} and the significant wave height (HS) was ~9 m.

* Correspondence to: Andrew T. Cox, Oceanweather Inc., 5 River Road, Suite 1, 06807 Cos Cob, CT, USA. E-mail: andrewc@oceanweather.com

†Deceased

The spectral description of sea state has been extended to underdeveloped seas and complex seaways (e.g. the JONSWAP and Ochi-Hubble spectral forms). However, even today wave spectral measurements over the open oceans are rare as almost all Metocean buoys equipped with wave recorders are moored along the continental margins. The need for more complete open sea wave climate specification is, therefore, increasingly satisfied by reliance on long-term simulations utilizing numerical wave spectral hindcast models adapted to individual ocean basins (Swail and Cox, 2000) and to the entire globe (Cox and Swail, 2000). Over the past three decades, hindcast databases have become increasingly used to derive design waves associated with 100-year and greater recurrence intervals using the statistical process of extremal analysis (e.g. Muir and El-Shaarawi, 1986).

1.2. Impact of very extreme sea states (VESS) on vessels

While the statistical approach to the specification of ship responses, such as heave, pitch, yaw and roll, has been gradually extended, at least in principal, to specification of wave-induced forces, bending moments and added resistance of a ship in a seaway, there has also been increasing focus on the risk to vessels encountering VESS. This has been highlighted in recent years by highly publicized losses such as the sinking of M.V. Derbyshire in a North Pacific typhoon (Faulkner, 2001), the spectacular container vessel damage to APL China attributed to parametric rolling in storm seas (France *et al.*, 2003), accidents with subsequent pollution of coastal areas such as Tanker Prestige (Lechuga, 2006) and media publicized passenger vessel encounters with extreme waves associated with injuries and ship damage, such as the several damaging encounters of Queen Elizabeth II with fierce NATL storms (e.g. Gyakum, 1983). It is estimated that about one third of major ship accidents are caused by ‘heavy weather conditions’ with such incidents often attributed to encounters with ‘anomalous’, ‘rogue’ or ‘freak’ waves (Monbaliu and Toffoli, 2003 and the follow-up study Toffoli *et al.*, 2006), though not all such accidents are associated with rogue waves (e.g. parametric rolling is caused by a different sea state encounter phenomenon).

While there is no rigorous definition of what constitutes an anomalous wave, there appears to be an emerging consensus that an anomalous wave has a crest-trough height (HM) ratio to HS of HM/HS > 2 and/or a crest height (HC) ratio HC/HS > 1.3 (e.g. Guedes Soares *et al.*, 2003). Recent analysis of a large field dataset suggests that these ratios are commonly attained or exceeded in low sea states (Bitner-Gregersen and Hagen, 2004; Christou and Ewans, 2011) wherein they do not have as much impact as the rarer occurrences high sea states. There are apparently only a handful of rogue waves in high sea states that have been instrumentally sampled, most of them in the array of well-instrumented offshore platforms in the North Sea, including the ‘Draupner’ wave at Draupner platform (HM = 25.6 m, Haver and Andersen, 2000) and the ‘Andrea’ wave at Ekofisk platform (HM = 22.9 m, Magnusson and Donelan, 2012). There is also an emerging consensus that except for the special class associated with interaction with high-current boundaries, rogue waves and crests, are favoured when the directional wave spectrum acquires a shape in frequency that implies high significant wave steepness, while at the same time the directional spreading narrows, especially near the peak frequency (Socquet-Juglard *et al.*, 2005, Onorato *et al.*, 2009; Waseda *et al.*, 2009; Toffoli *et al.*, 2010 Bitner-Gregersen and Toffoli, 2012). Because there is no reason to believe that rogue waves do not occur in high sea states, then the higher the background sea state as gauged by HS, the greater the potential for damage to a vessel or structure by a rogue wave or crest. In a sea state with HS ~ 14 m with properties conducive to production of a rogue wave, a wave with height of at least 28 m might be encountered. In a sea state with HS ~ 18.5 m, which was the world record high *in situ* (ship born accelerometer) measured HS, reported as the ‘Rockall Trough’ wave by Holliday *et al.* (2006), until the K-5 buoy in the eastern North Atlantic recorded a new highest measurement of HS – 19.0 m on 4 February, 2013, a rogue wave of 24 m or more might occur when assuming the existence of rogue waves in these sea states. In this study, we report several cases of satellite altimeter estimates of HS ~20 m, in which a rogue wave of ~40 m or more and a crest height of ~24 m of more might occur.

In an attempt to standardize terminology, the term ‘VESS’ has been introduced (Soares and Swail, 2006) to describe a sea state with HS above a threshold of 14 m. A sea state of this magnitude is rarely sampled in the *in situ* network of buoy and platform-mounted sensors, which as noted above lie mainly along the continental margins, and is comparable to design level sea states (return period of ~50–100 years) in most active areas of offshore resource production. Indicative of this interest is the recently established World Meteorological Organization (WMO)–Intergovernmental Oceanographic Commission (IOC) Joint Technical Commission for Oceanography and Marine Meteorology (JCOMM) initiative to establish a community database of VESS occurrences. The recent European Union (EU) MaxWave project (Rosenthal and Lehner, 2008) and the CREST Joint Industry Project (Buchner *et al.*, 2011) have addressed the incidence and causes (e.g. Garrett and Gemmrich, 2009; Waseda *et al.*, 2009) of occurrences of extreme individual crest heights and wave heights, the most impactful of which will tend to occur within VESS. The new EU ‘Extreme Seas Project’ has aimed to develop technology and methodology that need to be part of design for ship safety in extreme seas (see Bitner-Gregersen and Toffoli, 2012; Guo *et al.*, 2013). The project objective has also been to propose warning criteria for extreme sea states for marine structures. A recent workshop ‘Improving Wave Observations, Maritime Safety and Ship Design’ (Geneva, 4–5 October, 2011) organized by the EXTREME SEAS project and WMO brought together marine designers, ship operators, classification societies, insurance companies and ocean observation programmes of WMO and numerical wave modelling with the purpose to enhance safety of the future merchant fleet in extreme seas and abnormal conditions through implementation of the EXTREME SEAS results. Focus was given to acceptable safety levels and possible amendments of rules and regulations in IACS/IMO.

1.3. GlobWave satellite altimeter database

In this article, we investigate the global occurrence of VESS using a newly produced global database, called GlobWave, of historical estimates of HS made by satellite-mounted altimeters. A great advantage of such a database, of course, is that it is the only way to provide essentially uniform coverage of global shipping routes (except perhaps for emerging high Arctic routes) leading to reliable knowledge on distribution, frequency and ultimate severity of VESS and may also provide a basis for the distribution of extreme maximum individual wave heights and their properties, assuming as noted above the existence of rogue waves in VESS. The satellite altimeter record now spans over two decades, which is coincidentally about the same as the design lifetime of vessels, typically 20–25 years. GlobWave plays a critical dual role in this study. Not only does it provide a new assessment of global distribution of VESS and insight into storm types responsible for their generation, but it provides a source of validation of long term hindcast databases and a means to improve their accuracy at the upper end of the naturally occurring range of sea states. In this study, a new multidecadal hindcast database is combined with a new PC-based on-board voyage planning tool called VVOSS (Chen *et al.*, 1998) to simulate voyages along major trade routes selected to provide a conservative assessment of long-term risk of encounter of VESS.

1.4. Organization of article

This article is organized as follows. Section 2 gives the results of our scan of over two decades of satellite altimeter estimates of HS (and associated wind speed, WS) in terms of the geographical distribution of VESS events for thresholds of HS between 14 and 18 m. A summary is also given of the properties of extratropical cyclones (ETCs) that typically generate VESS. Section 3 describes the results of a numerical simulation of the risk of encounter of VESS by typical merchant vessels along a few major shipping lanes. Section 4 gives discussion and conclusions.

2. Satellite altimeter detection and global distribution of VESS

2.1. Basic principal of measurement

The estimation of HS by a satellite altimeter is basically a by-product of the analysis of the return pulse of centimeter wavelength radar energy emitted by the instrument toward nadir whose primary purpose is to determine the distance from the satellite to the sea surface by measuring the round-trip time. Information on sea state is contained within the slope of the leading face of the amplitude of the return signal, which is proportional to HS, while information on wind speed is contained within the strength of the return pulse relative to the power transmitted (so-called backscatter coefficient). The typical altimeter signal 'footprint' on the sea surface is a quasicircular pattern of a few kilometers in diameter. Altimeter measurements are typically averaged over 1-s (1-Hz sampling) to reduce signal noise, but the footprint size still yields a slightly noisy HS estimate, which is readily reduced by some along track binning to yield estimates with stability comparable to HS estimated by *in-situ* wave sensors. The radar signal is not actually 'measuring' wave height, and HS is retrieved by an algorithm based on linear regressions between return slope and HS derived from comparisons of large data sets of collocated and nearly simultaneous altimeter and *in-situ* buoy estimates of HS. The proof of concept of satellite altimetry was achieved with the SKYLAB, GEOS 3 and SEASAT missions in the 1970s. In the late 1980s, the Geosat mission provided the first long-term series of measurements. At least one satellite altimeter has been in operation since 1991. Orbital characteristics generally limit coverage to ~80 N in the Northern Hemisphere (NH) with sea ice and the Antarctica land mass limiting coverage in the SH. A comprehensive description of satellite altimetry and applications may be found, e.g. in Chelton *et al.* (2001). The satellite altimeter wave database has proven to be very useful to reveal systematic differences between the wave measurements of individual *in-situ* wave systems operated by different countries. This has led to the JCOMM 'Pilot Project on Wave Measurement and Evaluation and Test (PP-WET)' (see www.jcomm.info/WET).

2.2. GlobWave altimeter data set

GlobWave provides a new, homogenized, quality controlled, single point of access database containing virtually the entire record of satellite altimeter HS and WS measurements. This study applied only data from 1991 onward during which there has been continuous coverage by at least one satellite altimeter and includes the following missions: ERS1 8/1/1991–6/2/1996; ERS2 5/15/1995–5/11/2009; ENVISAT: 9/27/2002–12/7/2009; TOPEX: 9/25/1992–10/8/2005; JASON-1: 1/15/2002–3/3/2010; JASON-2 7/4/2008–3/3/2010 GEOSAT FO (GFO): 1/7/2000–9/7/2008. Figure 1 shows that since 1991 the number of simultaneous missions has ranged from just one in 1991 to five during much of 2002–2005. The native format of the data is netCDF time sorted, all missions combined. For this study, the data set was processed to separate monthly files sorted by altimeter.

The database is described in a general way in the Wave Data Handbook for GlobWave (Ash *et al.*, 2011). More details on the quality control procedures and calibration of the data streams from the various missions are given by Queffeulou and Croize-Fillon (2010) (QC2010). They describe a series of mission-dependent quality tests that were applied to produce a set of quality flags for each estimate, followed by additional filters applied to data near coasts, in so-called sigma0 blooms (Thibaut *et al.*, 2007),

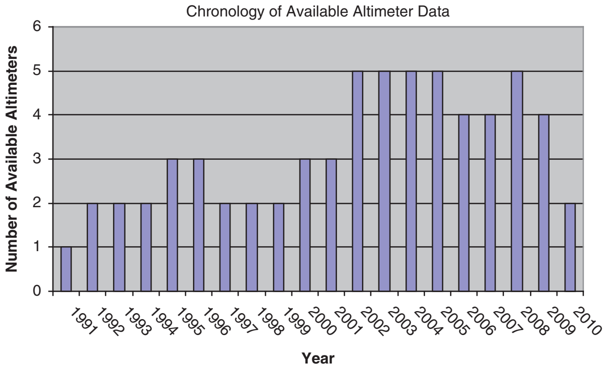

Figure 1. Number of altimeter missions in GlobWave database by year.

and to filter excessive changes between successive 1 Hz estimates along track. Individual estimates indicated by land and sea masks to be contaminated by sea ice or land were also eliminated. QC2010 also revisited the critical issue of calibration of the altimeter radar return – HS algorithm and updated the regressions for each mission based on comparisons of the altimeter measurements against worldwide buoy wave measurements. The standard error of the HS estimates overall is considered to range from about 0.8 m at HS ~4 m to about 1.7 m at HS ~12 m. Except for ERS1, and in the data range of most of the altimeter-buoy comparisons (HS < ~8 m) the mean differences between the recalibrated altimeter HS and the buoy HS comparisons data sets are within ±0.25 m and vary by mission, but there remain issues with regard to the extent to which the buoy data sets themselves can be considered to be unbiased.

2.3. VESS detection

The analysis searched for basin-specific orbit segments with a peak HS > 14 m in the 1 Hz data stream. By basin specific, we mean orbit segments within a major ocean basin, each defined by specific latitude–longitude ranges (note, however, to account for sampling variability and possible bias, we lowered the threshold to 12 m in the extraction process). The objectives of the analysis were to identify and remove any remaining spurious spikes from this data set, to summarize the spatial distribution and range of those occurrences by basin and mission, to distill the occurrences into parent storms, and to extract associated meteorological characteristics of the parent storms from global reanalysis data products and remotely sensed surface marine wind data. A preliminary analysis was reported by Cardone *et al.* (2011). Only data samples flagged as 'probably good measurement' in the GlobWave data stream are retained, where 'probably good measurement' is a somewhat subjective judgment of data quality assigned by the GlobWave project.

Orbit segment peaks were first identified objectively using a 'peak-finder' algorithm that follows the orbital data flow and seeks the absolute maximum of HS in the 1 Hz stream that is unique with respect to a specified along track distance window (set to 400 nm) and time window (set to 5 min). For each so identified orbit segment, a 15-min orbital slice centered on the peak was plotted as shown in Figure 2, which also for reference displays the closest hourly analysis of wind speed and sea level pressure in a 30° latitude–longitude box centered on the orbit. The source of the wind field and pressure fields is the new US National Oceanic and Atmospheric Administration (NOAA) Climate Forecast System Reanalysis (CFSR) atmospheric reanalysis (Saha *et al.*, 2010), which also serves as the basis of a new global wave hindcast database described below, a snapshot of which is also shown in Figure 2. This example plot is in fact of the orbit segment that transected the intense storm of 18 March 1999 near the International Dateline in the central North Pacific Ocean (NPO) that exhibited the highest 1 Hz HS found in the entire scan at 20.63 m. After median filtering of the data stream (median filtered along track HS are shown as '+' signs on the plot) over a 50-km orbital slice centered on the 1-Hz peak, this is reduced to 19.09 m. The hindcast peak (the hindcast method will be described in more detail in Section 3, but we note here that both CFSR forcing grid and the wave model grid have grid spacing of 55 km) is a little lower at 17.96 m but otherwise tracks the orbital trace of HS extremely well over the entire domain shown. The maximum CFSR wind speed at the point of maximum HS is 31.4 m s^{-1} but at the core of the storm wind field maximum just west of the altimeter track is 37.6 m s^{-1}. The model peak wind speed is about 10 knots higher than the altimeter wind speed and this is consistent with the tendency of altimeter winds to be biased low at high wind speeds for most altimeters.

Of the 5320 orbital segments found in this way with peak HS > 12 m, further QC led to the rejection of only 64 (~1.2%) as representing either spurious spikes or ambiguous cases near an ice edge. The distribution of the final population of 5256 peaks by altimeter and basin, along with relative percentages, are provided by Tables 1 and 2, respectively. Table 1 shows that the Southern Indian Ocean (SIND) contains the most cases at 32% and the South Atlantic Ocean (SATL) the least number of peaks at 7%. The NATL includes 26% of the cases, which is remarkable considering that the NATL basin is about a factor of three smaller in extent at mid-latitudes than the SIND. Table 2 shows the distribution of peaks by basin and HS ranges (HS > 12 m, HS > 14 m, HS > 16 m). For the latter two classes, the NATL now leads the occurrences on an absolute basis over all other basins. The four panel plot in Figure 3 shows the global distribution of peaks from all altimeters combined and for three ranges of VESS. A labor-intensive search for cases associated with tropical cyclones found only 147 peaks >12 m (<3% of the data). Only five of these samples had HS >16 m. Certainly, VESS have been documented to occur in tropical cyclones worldwide in the *in-situ* and platform-measurement record (e.g. Jensen *et al.*, 2006; Chao and Tolman, 2010) but it is difficult for an altimeter to 'see' an extreme sea state in a tropical cyclone mainly because the small scale of the area of

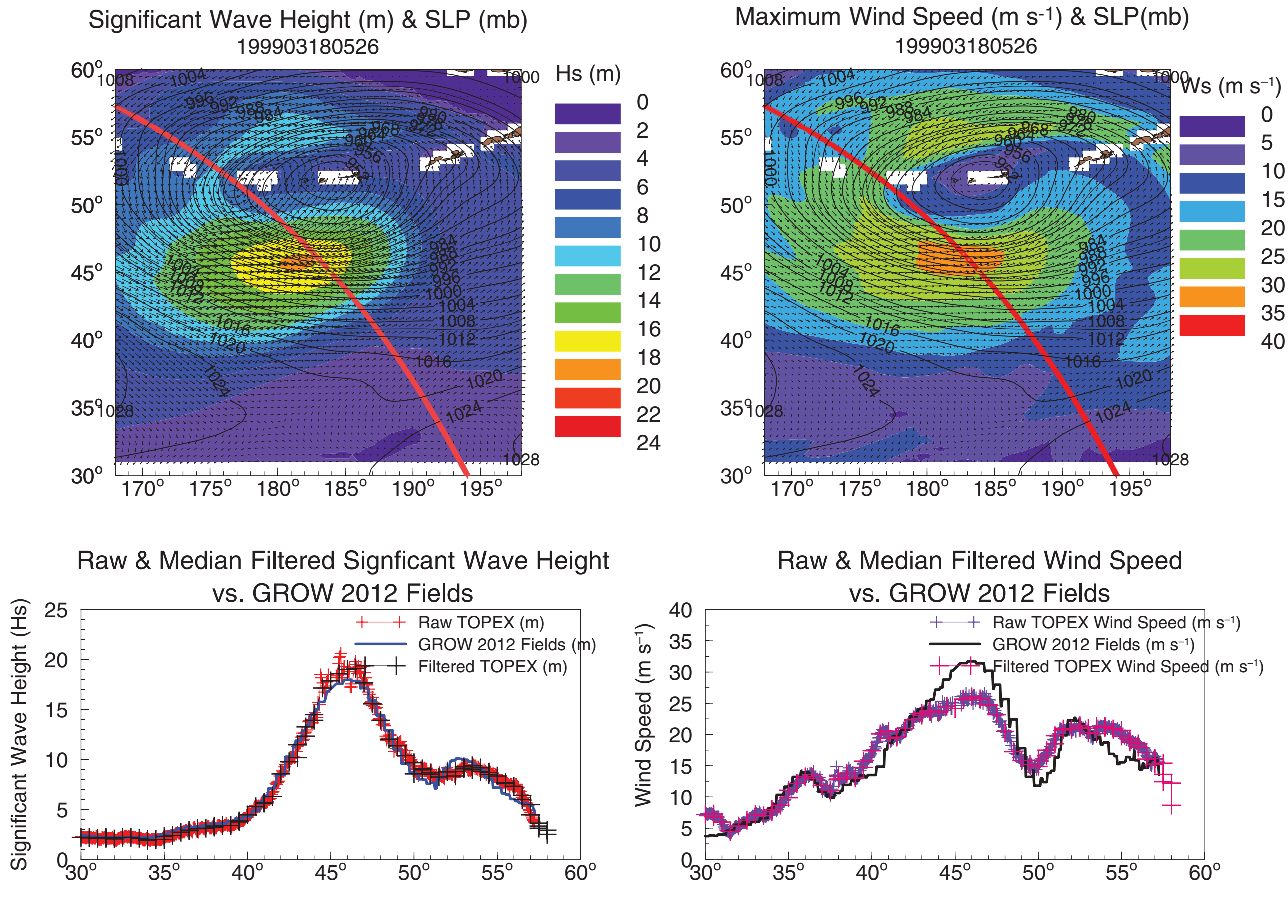

Figure 2. (Above row) Example plot of storm centered CFSR driven hindcast HS field (left) and surface wind field (right) superimposed on CFSR isobar analysis; (below row), TOPEX HS (left) and WS (right) storm transects (as plotted above), raw and filtered, compared to CFSR wind speed and CFSR-based wave hindcast, for the North Pacific VESS peak of 20.6 m on 199903180526 UTC.

Table 1. GlobWave distribution of orbit-segment peaks of HS >12 m (counts and relative percentage occurrence) sorted by altimeter mission and basin.

Satellite	NATL	%NATL	NPAC	%NPAC	SATL	%SATL	SPAC	%SPAC	SIND	%SIND	Total	%Total
ERS1	130	9.67	83	8.37	41	11.71	85	9.54	167	9.95	506	9.63
ERS2	246	18.29	180	18.15	39	11.14	81	9.09	162	9.65	708	13.47
TOPEX	404	30.04	301	30.34	97	27.71	290	32.55	495	29.50	1587	30.19
ENVISAT	146	10.86	106	10.69	53	15.14	117	13.13	239	14.24	661	12.58
GFO	160	11.90	165	16.63	59	16.86	138	15.49	299	17.82	821	15.62
JASON1	223	16.58	144	14.52	54	15.43	154	17.28	273	16.27	848	16.13
JASON2	36	2.68	13	1.31	7	2.00	26	2.92	43	2.56	125	2.38
Total	1345	25.59	992	18.87	350	6.66	891	16.95	1678	31.93	5256	100.00

peak sea states in such systems makes the chance scanning of the inner core of tropical cyclones by satellite-mounted nadir pointing altimeters very rare. Also, heavy convective rain in the inner core would tend to cause the radar beam to fail to properly sample the wavy surface. For these reasons, VESS in tropical cyclones are considered to be well under-sampled, hence the focus of this article is VESS generated in ETCs.

2.4. VESS storms

The distillation of the individual orbital peaks to a population of high-ranked associated ETCs was a two-step process. First, to keep this part of the study tractable, the threshold of peak HS was raised to HS > 16 m, which as indicated in Table 2 includes 185 cases. Second, the 185 candidate orbits were distilled to a unique set of storms by scanning the orbital plots together with associated weather map sequences, thereby identifying the often several orbits that transected the same storm at different locations and different times in its life-cycle. To aid this distillation, both the CFSR wind fields and the new deep-water global wave hindcast (Cox and Cardone, 2011) on a 70-km grid forced by CFSR winds were colour contoured and displayed together with each of the 185 orbital segments containing a peak HS >16 m. This new global hindcast is discussed in more detail in Section 3. Figure 4 shows such a plot

Table 2. Distribution of orbit segment peaks (counts and relative percentage occurrence) sorted by basin for indicated HS thresholds.

HS (m)	NATL	%NATL	NPAC	%NPAC	SATL	%SATL	SPAC	%SPAC	SIND	%SIND	Total	%Total
>16	65	4.83	34	3.43	6	1.71	15	1.68	65	3.87	185	3.52
>14	310	23.05	222	22.38	58	16.57	138	15.49	318	18.95	1046	19.90
>12	1345	25.59	992	18.87	350	6.66	891	16.95	1678	31.93	5256	100.00
Maximum HS (m)	20.24		20.63		16.57		17.51		18.84			

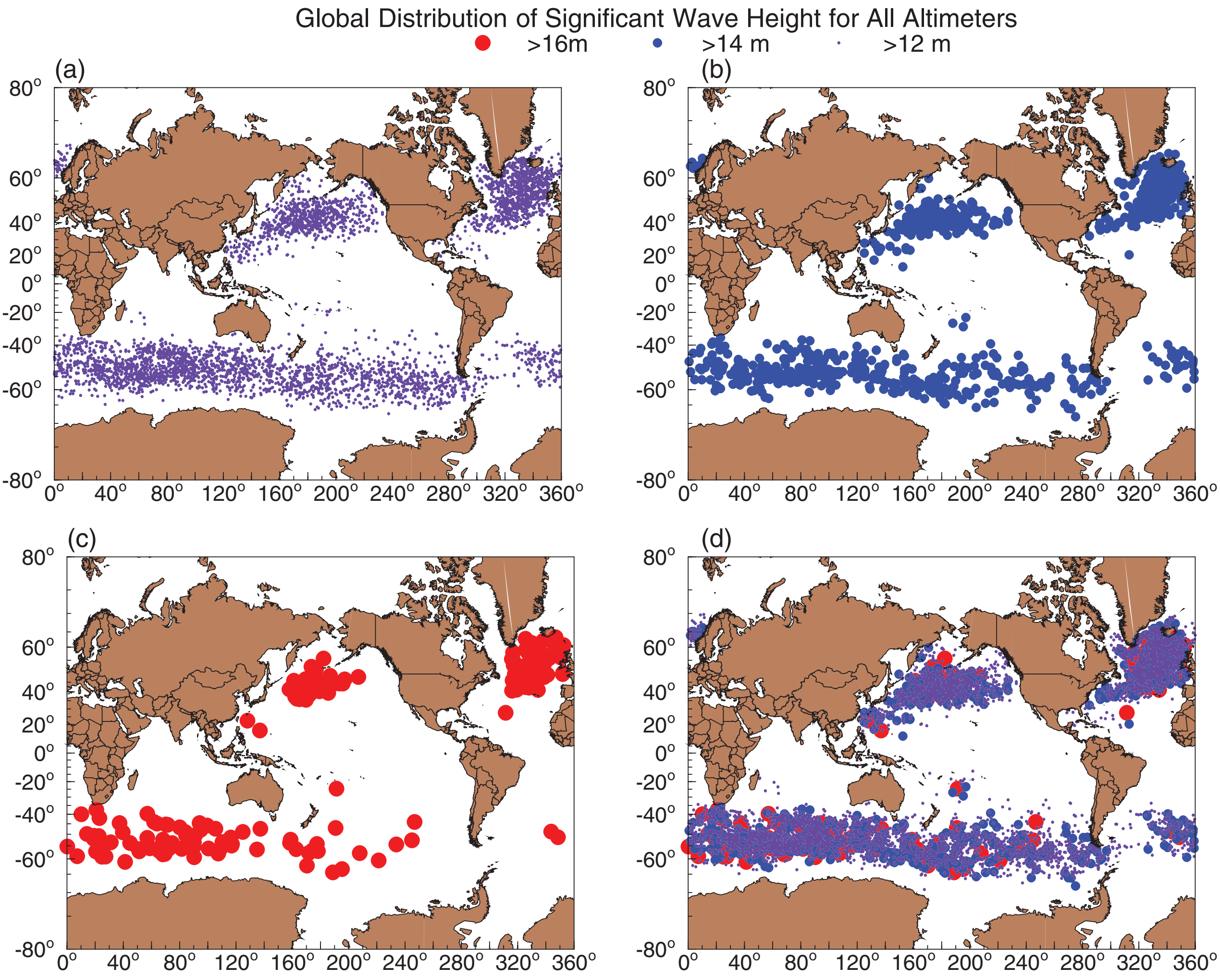

Figure 3. Plots of global distribution of GlobWave HS basin specific orbit segment peaks: (a) 12–14 m, (b) 14–16 m, (c) > 16 m, (d) all peaks.

for the top-ranked NATL storm of 10 February 2007, in which peak 1 Hz HS from GFO is 20.24 m. The storm responsible for this peak and a storm within the same week responsible for a comparable peak (1 Hz HS of 19.15 m) are also discussed and hindcast in Cardone *et al.* (2011). Note that the CFSR wave hindcast is quite skillful overall with only the part of the storm very near the core of the peak under-predicted slightly with a median measured peak HS of 18.95 m *versus* the hindcast of 18.33 m. Peak hindcast wind speeds are in the 35–40 m s^{-1} range for this storm (GFO does not provide altimeter wind speed). Figure 5 is a corresponding sample of a statistical comparison of the hindcast and the altimeter data for this orbit, which indicates for hindcast *versus* altimeter HS a correlation coefficient of 0.98, scatter index (ratio of standard deviation of the difference between the measurements and the hindcast and the mean of the measurements in the comparison sample) of 0.14 and bias of 0.27 m. Further evidence of the skill in this hindcast is given in Section 3.

The population of 185 peaks was ultimately distilled to a population of 120 individual storms consisting of 116 extratropical storms and 4 tropical cyclones. We had expected that the detection rate of these VESS storms would increase over time because the number of altimeter missions generally increased from an average of 2.25 missions in space at any given time during the decade of the 1990s (or the period 1992–1999 to be more precise) to an average of 4.63 missions during the period 2002–2009. Despite this nearly doubling of altimeter sampling, we find about the same global frequency of VESS storms per year

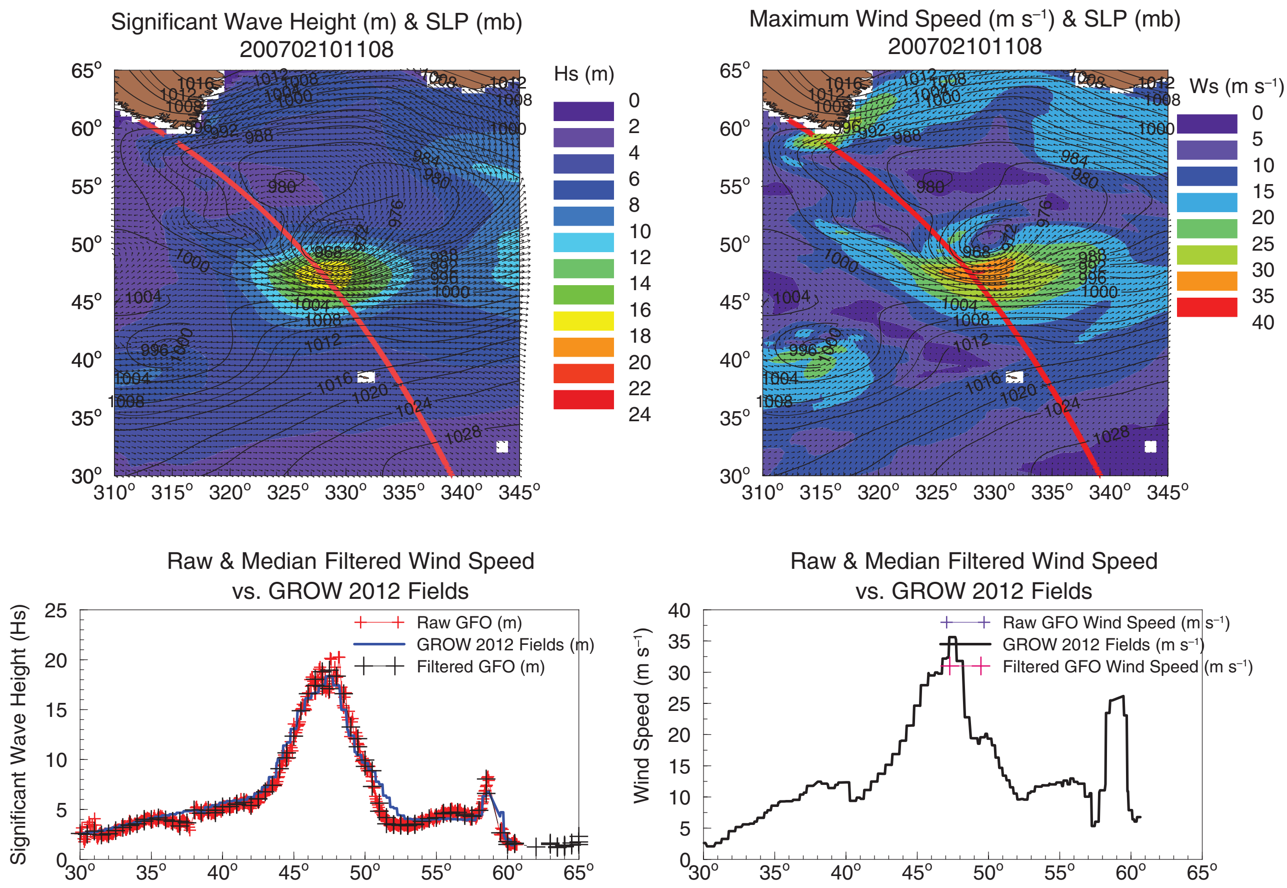

Figure 4. (Above row) Plot of storm centered CFSR-driven hindcast HS field (left) and surface wind field (right) superimposed on CFSR isobar analysis; (below) GFO HS (left) and WS (right) storm transects (as plotted above), raw and filtered, compared to CFSR wind speed and CFSR-based wave hindcast, for the highest-ranked VESS (20.2 m) North Atlantic storm of 10 February 2007.

in both periods at about five storms per year. However, we cannot claim on this evidence that the scan has found all VESS storms during this period and it is very likely that the actual storm frequency is higher. Also, it has been noted (Carter, 2011) that the GlobWave QC procedures may have invalidated some of the high-wave events recorded by Jason-1 and Envisat though we find no significant differences between the number of VESS events for these missions and the other missions after mission duration is considered. Table 3 gives the date, location and peak HS and WS of the top five events in each basin.

Cardone *et al.* (2011) have reported on a preliminary analysis of the key VESS storm properties as averaged over the highest ranked VESS storms based on small samples of storms for which detailed meteorological reanalyses were carried out (i.e. storms with peak VESS of HS >16 m). These properties are in turn sorted by major basin in Table 4, which gives minimum central pressure, deepening rate, cyclone translation speed, the kinematically reanalyzed peak wind speed (equivalent 30-min average at 10-m elevation) and the minimum distance between the track of the center of cyclone minimum sea level pressure and the track of the wind-speed maximum (so-called surface wind jet-streak) that propagates typically with the speed of the parent low center and on its equator-ward flank. This minimum distance, dubbed here R_{max} for radius of maximum wind speed, tends to occur near the time of maximum storm intensity.

A more detailed description of the meteorological properties of VESS ETCs will be reported by Cardone *et al.* (in preparation). Briefly here, the most striking characteristic of the VESS ETCs is a roughly 24-h period of 'explosive deepening' making these storms of the class first described by Sanders and Gyakum (1980) who defined such rapid intensification as a fall of central pressure of at least one Bergeron (defined as a pressure drop of at least 1 mb h^{-1} maintained over at least 24 consecutive hours referenced to 60° latitude). The VESS 'bombs' intensify more typically at a rate of 1.5 Bergerons (at 45° latitude, a deepening of 33 mb in 24 h corresponds to 1.5 Bergerons). R_{max} typically migrates inward to within ~2° of the pressure center in NATL and NPAC storms and within 2°–4° in SIO storms as the peak wind speed increases to super-Beaufort speeds (>33 m s^{-1}) with 40 m s^{-1} not unusual especially in NATL and NPAC storms. There is rapid growth of peak VESS from its background level to HS >12 m in the vicinity of the jet streak maximum during the period of maximum deepening. The storm translation speed tends to lie between 15 and 20 m s^{-1}. This deepening stage is followed by a fairly brief period of ~12 h of quasiequilibrium

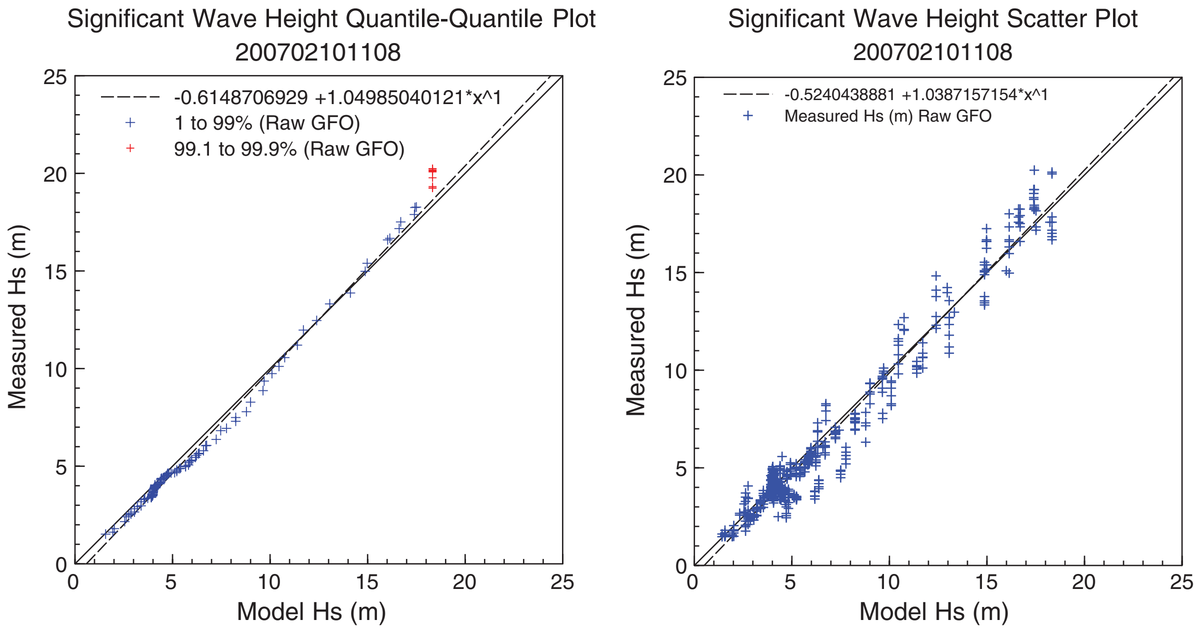

	Number of Pts	Mean Meas	Mean Hind	Diff (H-M)	RMS Error	Stnd Dev	Scat Index	Ratio	Corr Coeff
Sig Wave Ht (m)	560	6.35	6.62	0.27	0.93	0.89	0.14	0.68	0.98

Figure 5. CFSR-driven wave hindcast quantile–quantile plot (above left) and scatter plot (above right) and difference statistics (below) for HS (m) for the top-ranked NATL storm of 10 February 2007.

stage of maximum intensity with respect to minimum central pressure, magnitude and location of maximum wind speed but with slow continued increase in peak VESS to its storm peak value, which is followed by a storm decay stage of duration ~ 24–48 h within which the central pressure rises rapidly, the peak wind speed and peak sea states decrease rapidly and the radius of maximum wind speed increases gradually as the overall storm circulation expands. The relative brevity of the period of VESS within the full life cycle of intense marine ETCs (~12–24 h) operates to minimize the chance encounter of such potentially dangerous sea states by merchant vessels even if they do not avail themselves of weather routing services and this question is investigated more systematically in Section 3.

3. Simulation of VESS encounter probability along major routes

3.1. Voyage simulator

This section describes the application of a voyage simulator together with a new global multidecadal hindcast to estimate the rate of encounter of VESS by merchant vessels plying several common trade routes. The voyage simulator, described by Chen *et al.* (1998), is called TOWSIM because it was first applied to evaluate conditions to be expected along transocean tows. However, it may also be applied to merchant vessels by simply adopting an appropriate vessel speed in lieu of a tow speed. The route is specified by a departure port, an arrival port and a set of way points with great circle or rhumb line navigation between each waypoint. The voyage simulation recreates voyage weather conditions as those prescribed by the hindcast database. Typically, a vessel departure is initiated every 6-h for the 33 years (1979–2011) covered by the hindcast database, resulting in a total of up to 48 180 simulations if the full period and all months are simulated. Once the simulation of a voyage starts, the vessel sails along the prescribed route. Along the way, environmental conditions (winds and waves only) are retrieved from the hindcast data base according to dead-reckoned positions every 6 h. In its full capability, data such as total route distance, route travel time, vessel motions, including roll and pitch, wind speed and wave height encountered, fuel consumption and other results may be saved. For this study, neither vessel responses nor speed reductions due to sea states encountered were considered and only bulk wind and wave parameter results were saved. The wind and wave encounter samples were formed into various joint probability density functions and exceedance probabilities and stratified by month of departure. What is of most interest here is the duration of encounters of VESS threshold sea states over the life of the vessel for typical usage.

3.2. GROW 2012

In order to most realistically reflect the risk of encounter of VESS on the high seas, the hindcast database must be skillful over the whole range of naturally occurring sea states, or at least exhibit small and correctable bias in the range of interest here. Achieving these properties in a continuous hindcast has been challenging. Most

Table 3. Top five-ranked altimeter detected storm peak sea states (1 Hz HS) in each basin with date and location and associated wind speed shown. Both raw 1 Hz peaks and corresponding median filtered peaks shown. Comparisons with the GROW 2012 hindcast peak is also shown.

Storm date	Lat.	Long.	Altimeter	Ws ($m\ s^{-1}$)	Raw HS (m)	Median filtered HS (m)	GROW 2012 hindcast HS (m)
North Atlantic							
200702101108	48.14	327.35	GFO		20.24	18.95	18.33
200702092131	48.65	341.45	JASON1	25.57	19.15	18.42	17.14
199502020709	50.75	326.56	TOPEX	22.89	19.1	17.31	15.75
200002081151	57.73	336.52	GFO	25.62	18.64	18.08	16.75
200302120845	48.25	319.5	TOPEX	25.42	18.27	18.07	15.35
Averages				24.88	19.08	18.17	16.67
South Atlantic							
199507180750	−51.36	348.57	TOPEX	22.73	16.57	15.73	13.29
199206060939	−55.33	0.25	ERS1	21.95	16.31	14.91	16.35
200205240919	−39.99	10.23	ERS2	25.14	16.19	15.38	14.27
200106232057	−59.03	7.24	TOPEX	25.29	16.12	15.61	14.94
200206112042	−48.8	343.77	GFO	21.7	16.03	15.62	14.50
Averages				23.36	16.24	15.45	14.67
North Pacific							
199903180526	45.61	183.4	TOPEX	25.95	20.63	19.09	17.96
199903212109	51.14	176.81	TOPEX	26.85	19.5	18.58	17.89
201001140622	42.84	167.13	JASON1	25.35	17.39	16.14	15.56
200602031141	40.79	178.3	JASON1	24.88	19.39	17.86	17.72
200802041046	37.2	162.01	ENVISAT	25.03	18.09	17.29	15.80
Averages				25.61	19.00	17.79	16.99
South Pacific							
200306010841	−56.87	174.25	GFO	22.24	17.51	16.52	16.89
199408141934	−60.55	221.3	TOPEX	23.05	17.41	16.89	14.93
199909120101	−54.47	233.84	TOPEX	25.42	17.35	16.43	15.78
199804230945	−57.89	207.85	TOPEX	24.72	16.66	15.93	13.79
200606140157	−44.06	246.79	GFO	22.17	16.59	16.17	15.54
Averages				23.52	17.10	16.39	15.38
South Indian							
200610090425	−53.59	110.36	GFO		18.84	18.35	16.94
200705130900	−39.71	57.04	JASON1	25.13	18.71	17.12	17.20
200809020748	−52.49	21.86	ENVISAT	24.67	18.18	16.45	14.52
199312042352	−51.5	116.3	TOPEX	22.03	17.83	17.1	14.83
199410140925	−56.09	100.48	TOPEX	24.28	17.83	16.89	15.76
Averages				24.03	18.28	17.18	15.85

Table 4. Average meteorological properties associated with storms with HS 16 m and greater stratified by basin.

Basin	Min. SLP (mb)	Max. deepening rate (mb 24 h^{-1})	Max. surface wind speed ($m\ s^{-1}$)	Min. radius of max. winds (km)	Max. backwards 6-h storm trans. velocity ($m\ s^{-1}$)	Average backwards 6-h storm trans. velocity ($m\ s^{-1}$)
North Atlantic	947	39	37	198	27	17
North Pacific	952	35	35	239	26	16
South Indian	941	31	32	285	30	19
South Atlantic	943	34	34	256	27	16
South Pacific	940	31	27	265	27	19

attempts since the first such hindcast, known as the Global Reanalysis of Ocean Waves (GROW) reported by Cox and Swail (2000), while exhibiting good skill overall, tended to become increasingly negatively biased beginning at sea states as low as HS of ∼8 m. In fact, before 1999, when routine monitoring of surface marine winds on a global scale by the QuikSCAT scatterometer began, even hindcasts of individual storms driven by carefully reanalyzed wind fields tended to exhibit negative bias in storms with peak HS above 12 m (Cardone *et al.*, 1996). A more detailed description of GROW2012 and its validation are given by Cox and Wang (2013).

GROW2012 improves upon the first GROW effort (Cox and Swail, 2000) in the following significant ways: (1) atmospheric wind input time step and wind field and wave model grid spatial resolution are increased to 60 min and 55 km, respectively; (2) ice fields are updated daily, rather than monthly; (3) global tropical systems are included by inlaying for each historical cyclone along its 'best-track' within the period simulated, detailed solutions of the surface wind field made by a proven mesoscale planetary boundary layer model (Thompson and Cardone, 1996); (4) a proven third-generation model is employed (Khandekar *et al.*, 1994) with global shallow water effects included; (5) the wave-spectrum resolution is expanded to include improved spectral directional resolution (48 bands *vs*. 24 bands) and additional spectral frequency bands (25 *vs*. 23). The grid system covers the global oceans from 70° South latitude to 75° North latitude and output is available at an hourly time step. A large number of wave spectra are archived though spectra are not referred to in TOWSIM. To date, the 33-year historical period 1 January 1979–31 December 2011 has been run.

The GROW2012 hindcast has been intensively validated against world-wide wave measurements from deep-water buoys and from global altimeter measurements (Cox and Wang, 2013). Figure 6 shows the total of 101 buoy locations, mainly in the Northern Hemisphere, which were time-matched with the GROW2012 hindcast and compared. Locations were restricted to high-quality, deep-water sites at least two grid spacings from the coast. The *in-situ* validation consisted of nearly 9 million individual observations. Overall, the average HS difference between the hindcast and the buoy measurements is under 20 cm with a root mean square difference of 46 cm and correlation coefficient of 94%. Satellite altimeter wind and wave measurements provide a basis for global skill assessment and so measurements from the GlobWave project over the period 1991 to present were used in the validation. The median of all altimeter observations (typically measured at 1 Hz) within the 0.5° grid spacing ±30 min were considered a single validation point. Overall, there were just <633 million validation points with an average wave bias of <13 cm, root mean square error of 0.49 and correlation coefficient of 95%. Plots of wave bias on a global projection indicate that the vast majority of the global oceans have a mean wave bias <25 cm and wind bias <1 m s^{-1}. The small negative bias of GROW2012 in the VESS range of HS is revealed in Figure 7, which shows the mean difference between GROW2012 and altimeter HS in 1-m bins of 0.5-m width of satellite measurements over the full data range. The mean difference is within ±0.5 m over the bins centered on 0.25 m up to 14.75 m, which is remarkable considering the tendency (as noted in Section 2) for previous continuous hindcasts driven by atmospheric reanalysis products to exhibit considerable negative bias at much lower HS thresholds. In GROW2012, the negative bias does not attain ~1.0 m until HS ~17 m and in the highest bin centered on 19 m, it is −1.75 m, or <10% of the signal level. Stratification of this bias by major basin indicates that at the highest sea states (HS >16 m) the bias is least in the NPAC (~0.5 m), greater in the NATL (~1.0 m) and greatest in the Southern Oceans (~1.5 m). These small negative biases in GROW2012 in the upper VESS range are accounted for in the interpretation of the statistical output of TOWSIM below. It should be noted that the aforementioned JCOMM PP-WET project has produced some results that suggest that the uncertainties in buoy wave measurements (from which altimeters are calibrated) are of a similar level to the biases in the hindcast, especially at the higher sea states, so the biases may not be quite as large as stated herein.

3.3. Simulation results

There are hundreds of trade routes plied by the current merchant ship and tanker fleets. Rather than seek an exhaustive assessment of risk of encounter of VESS on all such routes, which would present an enormous computational burden within TOWSIM, we seek here conservative estimates of such risk by running the simulations for the nine

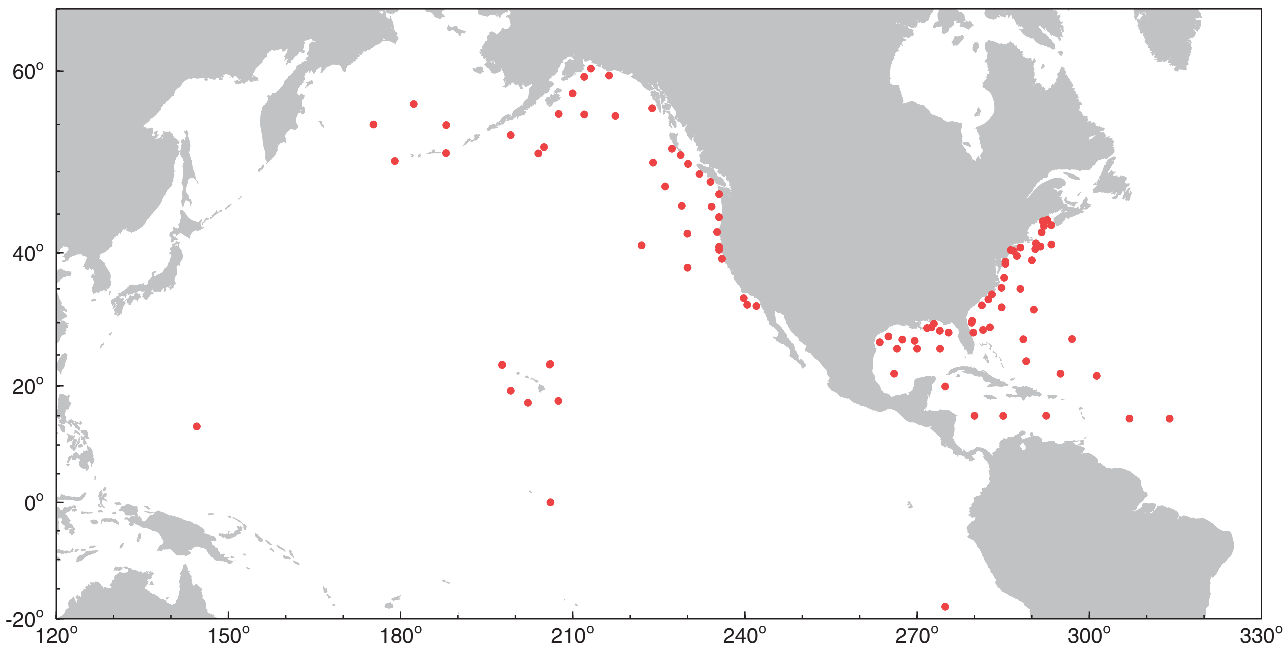

Figure 6. Buoy locations applied in GROW validation.

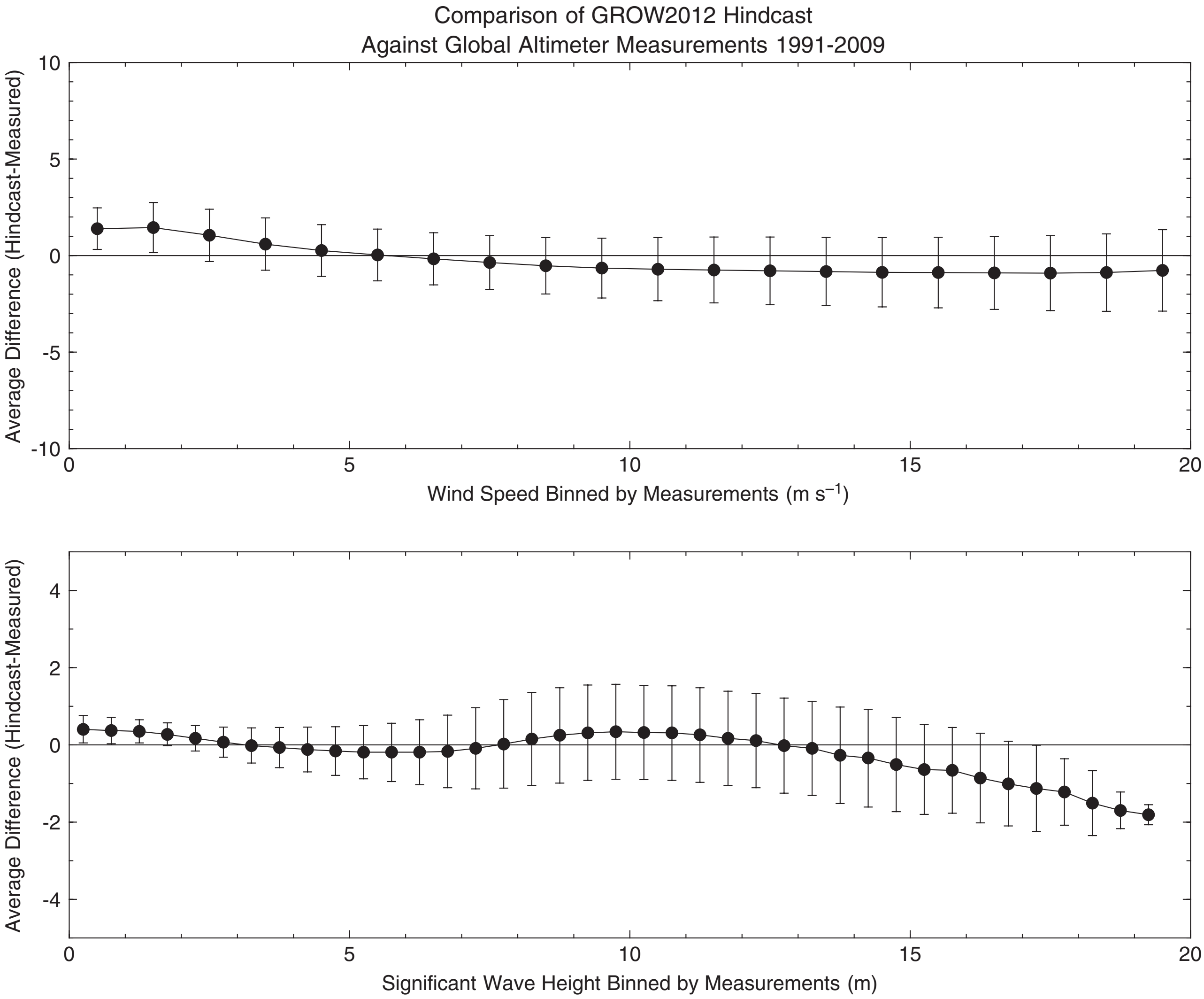

Figure 7. Average difference between GROW2012 and altimeter measurements (1991–2009) of significant wave height and wind speed in 0.5 m and 1 m s^{-1} bins of the measurements.

'indicative routes' shown in Figure 8. These routes traverse mainly the extratropical belts of the major basins. Exclusion of the routes that traverse mainly tropical regions is also justified as noted above, VESS in tropical cyclones are under sampled in GlobWave. Also, the hindcast database grid resolution is not optimal for resolution of such systems anyway. This simulation, therefore, addresses the risk of encountering the class of ETCs dubbed 'winter hurricanes' that generate VESS.

Figure 8 also summarizes the nine routes selected in terms of departure and arrival ports, distance travelled, selected vessel speed and resulting route duration. A vessel speed of 16 knots was specified for all routes. The three routes in the NATL and NPAC (two that approximate great circles and one a rhumb line) are within the envelope of commonly travelled routes in these basins. Real routes are, of course, often mapped before departure based on strategic weather guidance and other factors, and then adjusted tactically while underway to reflect changing weather forecasts. The encounter statistics derived here are, therefore, conservative with respect to a real operational environment, but they are also free of the 'fair-weather-bias' that afflicts Metocean statistics based on historical ship weather observations. The three Southern Ocean (SO) routes (all modified great circle routes) are even more idealized (except perhaps for Rio-Singapore) than their NH counterparts and laid out to ensure that the main clusters of VESS occurrences in the SIO, SPO and SAO are sampled.

A most basic output of TOWSIM is the bivariate distribution of HS and TP accumulated from the 6-hourly samples encountered over the entire ensemble of simulations for a given route and month of departure. Figure 9(a)–(c) shows examples of these distributions for the three routes that exhibited the most extreme monthly VESS encounters. Figure 9(a) shows the distribution in terms of the HS-TP scatter diagram for the NATL DB-BR route for January. The granulation in sampled TP is a result of the wave model spectral resolution, which becomes rather coarse at higher frequencies. Note that VESS sea states tend to be associated with TP in the range of about 14–18 s, with the only sea states with TP > 20 s associated with

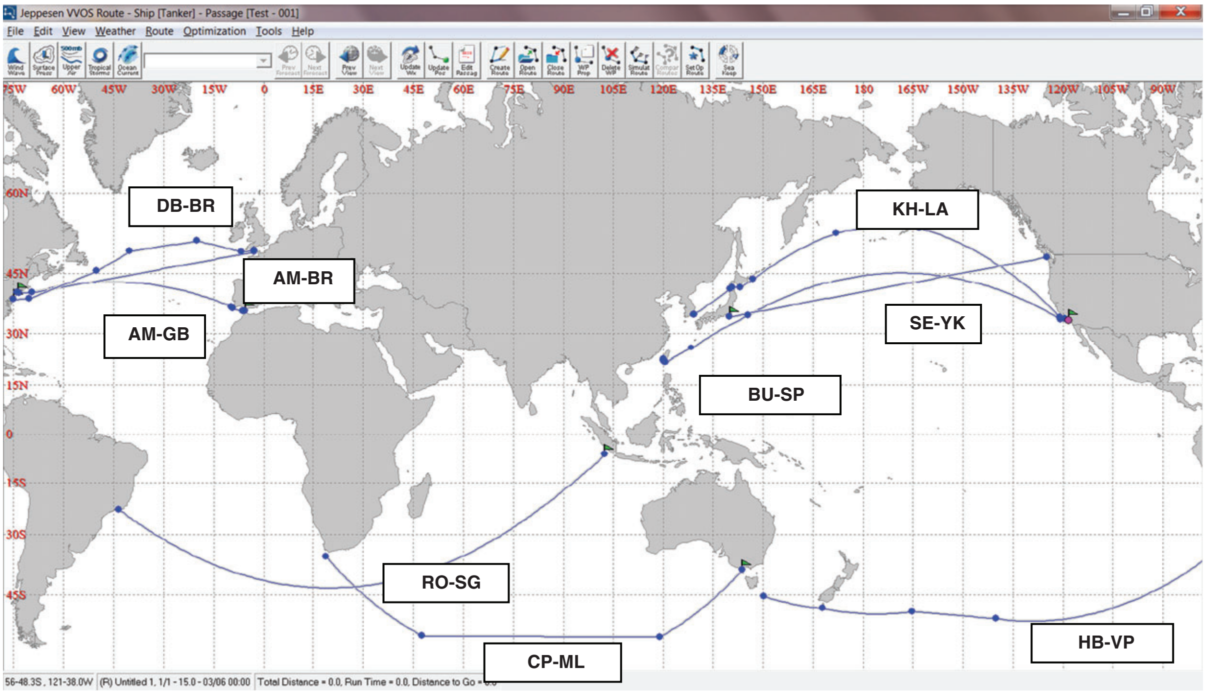

Ports	Distance (Nmi)	Speed (knts)	Time Hours
NORTH ATLANTIC OCEAN			
Delaware Bay - Bishop Rock DB-BR	3122.8	16	195.2
Ambrose-Bishop Rock AM-BR	3071.8	16	192.0
Ambrose –Gibralter AM-GB	3180.9	16	198.8
NORTH PACIFIC OCEAN			
Busan – San Pedro BU-SP	5292.2	16	330.8
Seattle-Yokohama SE-YK	4348.2	16	271.8
Kao-Hsiung – Los Angeles KH-LA	6168.3	16	385.5
SOUTHERN OCEAN			
Rio de Janeiro Singapore RO-SG	8134.6	16	508.4
Capetown - Melbourne CP-ML	5484.7	16	342.8
Hobart – Valparaiso HB-VP	5903.5	16	369.0

Figure 8. Nine trade routes along which encounter statistics simulated using TowSim with descriptions of each listed.

rather low HS and hence probably ‘swell’ sea states. Figure 9(b) gives the scatter diagram for the NPO YK-SE route again for January. There are considerably more TP > 20 s ‘swell’ encounters, as expected for this much larger basin; however, VESS remain constrained to the TP range of ∼14–18 s. Finally, we show in Figure 9(c) the SIND CP-ML route for July, which is the most extreme route found for the Southern Oceans. There are a seen here a few cases of ‘swell’ encounters with TP > 22 s.

Table 5 gives a summary for each of the nine routes of the ‘winter’ monthly exceedance probabilities (MEP) for HS thresholds of 5, 8, 11 and 14 m. For typical container vessels, vessel management needs tend to increase in a sea state of HS > 5 m. Above HS of 8 m the possibility of damage to cargo and vessel increases significantly and above 11 m, of course, sea state induced accidents become more common, while 14 m is the nominal VESS threshold. Given the reliability over a wide dynamic range

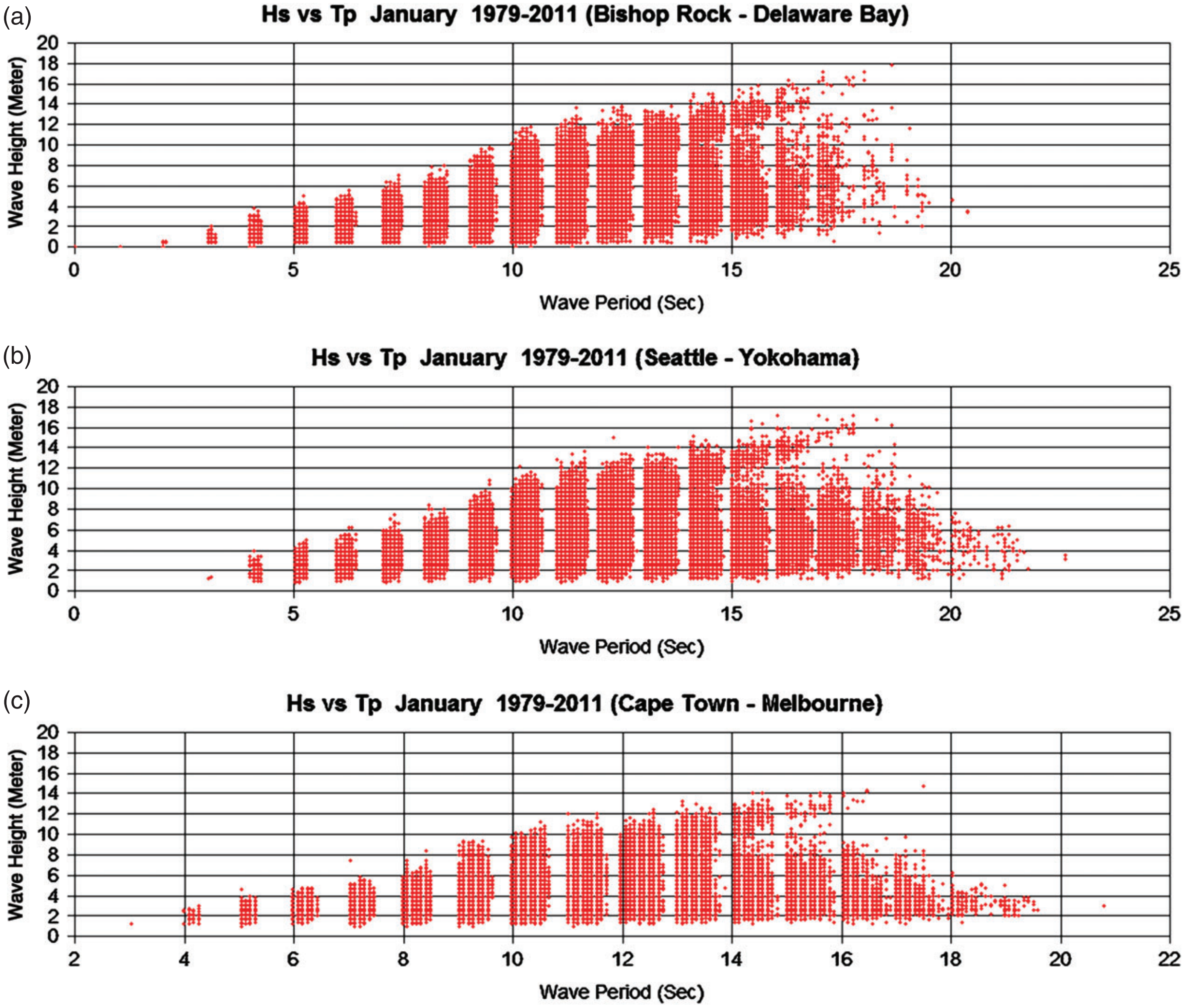

Figure 9. (a–c) Significant wave height (m) *vs*. peak wave period (s) for all Januaries from 1979–2011 for NATL DB-BR, NPAC SE-YK and SIND CP-ML.

Table 5. Exceedance probability (%) for HS thresholds of 5, 8, 11 and 14 m along nine trade routes on the basis of voyage simulations for 6-h departures through the 33-year GROW2012 global wave hindcast for the indicated month.

HS threshold (m)	North Atlantic Jan. DB-BR	North Atlantic Jan. AM-BR	North Atlantic Jan. AM-GB	North Pacific Jan. BU-SP	North Pacific Jan. YK-SE	North Pacific Jan. KH-LA	Southern Ocean Jul. RO-SG	Southern Ocean Jul. CP-ML	Southern Ocean Jul. HB-VP
>5	29.12	27.65	19.06	15.55	35.43	22.91	13.54	44.78	23.42
>8	5.95	5.18	2.91	1.70	5.71	3.38	1.07	6.80	2.80
>11	1.13	0.89	0.43	0.15	1.05	0.55	0.13	0.99	0.24
>14	0.07	0.05	0.02	<0.01	0.09	0.05	<0.01	0.04	<0.01

of HS in the GROW2012 hindcast as noted above, these probabilities did not need to be bias corrected. Table 5 indicates that at the 5-m threshold, MEP is highest, at 44.78% in the SO along the route that ventures south of 45° (HB-VP). The highest MEP for 5 m HS in the NH is for the YK-SE rhumb line route at 35.43%, while in the NA MEP for 5-m threshold is greater for the DB-BR route at 29.12%. At the 11-m threshold, the MEP are approximately the same at ~0.1% for these same routes in each basin, but for the VESS threshold of 14 m, the highest MEP are in the NPAC and NATL routes exemplified above at about 0.1%.

An alternative statistical distribution that is a standard output of TOWSIM is the monthly exceedance probability of the single maximum peak sea state to be expected for a simulated voyage for any month (MEPm). Table 6 gives this probability for HS >14 m. The highest single MEPm are found in the NPAC along the YK-SE route for the months of Dec., Jan. and Feb. at slightly >3%. The second most extreme route is the NATL DB-BR route with nearly

Table 6. Monthly and annual probability of exceedance of voyage maximum HS >14 m on the basis of simulated voyages through the GROW2012 wave hindcast on the basis of 6-h departures over 33 years for nine routes.

Month	North Atlantic DB-BR	North Atlantic AB-BR	North Atlantic AB-GB	North Pacific BS-SP	North Pacific YK-SE	North Pacific KH-LA	Southern Ocean RO-SG	Southern Ocean CP-ML	Southern Ocean HB-VP
Jan.	2.00	1.39	0.42	0.29	1.34	3.15	–	0.10	–
Feb.	2.31	2.55	0.54	0.08	0.51	3.11	–	0.35	0.08
Mar.	1.30	0.61	0.10	0.10	1.12	1.52	–	0.56	0.15
Apr.	0.05	0.13	–	–	0.15	0.35	–	0.88	0.08
May	–	–	–	–	–	–	0.17	0.66	0.10
Jun.	–	–	–	–	–	–	0.10	1.36	0.28
Jul.	–	–	–	–	–	–	0.07	1.54	0.22
Aug.	–	–	–	–	–	–	0.27	1.39	0.15
Sep.	0.05	0.15	0.08	–	0.38	0.20	0.08	1.26	0.08
Oct.	0.32	0.22	0.02	0.10	0.51	0.76	–	0.61	–
Nov.	0.98	0.71	0.20	0.31	1.54	0.93	0.10	0.25	0.08
Dec.	2.88	1.64	0.29	0.24	1.81	3.25	–	0.10	0.07
Annual	0.82	0.62	0.14	0.09	0.61	1.11	0.07	0.76	0.11

Table 7. Number of 6-h time step encounters of HS >17 m in bias-adjusted GROW2012 global wave hindcast along simulated voyages for 6-h departures over 33-years, total number of hours of encounter and total encounter for a vessel along the trade route for the maximum possible number of actual departures over a lifetime of 33 years.

Route	North Atlantic DB-BR	North Atlantic AB-BR	North Atlantic AB-GB	North Pacific BS-SP	North Pacific YK-SE	North Pacific KH-LA	Southern Ocean RO-SG	Southern Ocean CP-ML	Southern Ocean HB-VP
Counts for 1460 departures per year	55	38	8	0	23	34	2	95	5
Equiv. hours	330	228	48	0	138	204	12	570	30
No. instant turnaround departures per year	45	46	44	26	32	23	17	26	24
Hours of encounter in 33 years	10.2	7.2	1.5	0.5	3.0	3.2	0.1	10.2	0.5

3% exceedance in Dec. and >2% for Jan. and Feb. In no month and for no route in the SO does MEPm exceed 1.54% and this is for CP-ML in the month of July. We are left with the impression that while the SO are more likely to present sea states that present operational challenges, a vessel is more apt to be exposed to dangerous sea states along NATL and NPAC mid and high latitude routes.

But how apt is a vessel operating without the benefit of tactical weather guidance to encounter extreme sea states of such magnitude that they may yield rogue waves of catastrophic heights of the order of 40 m? Table 7 gives for each of the nine routes and only for the HS threshold of 17 m, the raw ‘counts’ over the 33 years and the equivalent number of hours of exposure. A ‘count’ is a 6-h sample of GROW2012 and we assume steady sea state conditions within each 6-h period. Before extracting these counts, the probability distributions were adjusted to account for the small basin-dependent negative biases in the GROW2012 HS hindcasts in this range as discussed above. The raw counts are, of course, based on departures every six hours, or 1460 departures per year and 48 180 departures in 33 years. On the basis of the mean voyage durations given in Figure 8, a most conservative estimate of the maximum number of actual voyages a given vessel can make in a year (or 33 years) can be made by assuming instant port turnaround. The annual number of such voyages is also given in the Table 7 and ranges from 17 voyages year^{-1} for the RO-SG route to 46 voyages year^{-1} for the AM-BR route. Normalizing for this factor, the mean number of hours of exposure to a vessel along each route during its entire 33 lifetime may be estimated conservatively and as given in the Table 7 ranges from <6-h (one sample) in six of the nine routes to a maximum of 10.2 h for the DB-BR NATL and the CP-ML SIND route. The CP-ML route distance, at 5485 Nmi, is 76% greater than the DB-BR route distance but no attempt is made to further normalize the risk of encounter for distance, because the data already indicate that from the standpoint of concentration of VESS, the NATL appears to be the harshest basin, followed by the NPAC, followed by the SO. This is a perhaps counter-intuitive result given the mariner’s anecdotal reputation of the harshness of the southern oceans but this result is in fact consistent with the outcome of the altimeter scan presented in Section 2.

4. Summary and conclusions

The impact of extreme sea states on marine infrastructure design and operations is the focus of intensive attention in the scientific and engineering communities at the present time. In this study, a new quality-controlled database of global satellite-derived estimates of significant wave height (HS) and surface marine wind speed from seven missions spanning the period August 1991–March 2010, known as GlobWave, was scanned to yield over 5000 ocean basin specific orbit segments with peak HS >12 m. This population was subsequently distilled to a population of 120 individual storms (so-called VESS storms), in which there was at least one altimeter estimate of HS >16 m. The highest HS were observed in the Northern Hemisphere with ten (four) orbits segments in the NAO (NPO) with a peak HS of >18 m. Only three HS peaks >18 m were seen in the entire Southern Oceans. Three of the >5000 orbit segments had a peak HS >20 m and none was >20.6 m, which is reduced to 19.1 m after median filtering. These estimates are based on the intrinsic altimeter sampling rate (generally 1 Hz). Smoothing or median filtering the data stream over a ~50-km orbit length reduces the peaks on average by about 0.9 m.

The number of VESS storms detected was found to be greatest in the NATL (the smallest basin) followed by the NPAC, SIND, SPAC and SATL. This appears to be consistent with general circulation studies of extratropical cyclogenesis, frequency and intensity in general atmospheric circulation models. For example, Brayshaw *et al.* (2009) found that North America has the ideal shape to enhance land-sea contrast and strength of baroclinicity leading to robust generation of intense cyclones over the North Atlantic basin as it provides an environment especially conducive to strong baroclinic instability. GlobWave has probably not allowed the detection of all VESS storms during its historical period but we do find a consistent detection of approximately five events per year on a global basis, suggesting that the detection rate of VESS storms is rather insensitive to the number of simultaneous missions for two or more simultaneous missions.

All but 4 of the 120 extreme VESS storms (i.e. with HS >16 m) detected were associated with ETCs. This reflects mainly the poor sampling of the small area of sea states in the inner core of tropical cyclones by satellite-mounted small-footprint nadir pointing altimeters rather than any intrinsic reluctance of intense tropical cyclones to excite VESS. The peak wind speeds (equivalent neutral wind speed at 10-m elevation) in the most intense VESS storms exceed 40 m s^{-1}, a speed which transforms using a prevalent gust model to a peak sustained 1-min wind speed (the reference interval used to classify hurricanes) of about 100 knots or 115 mph. This speed corresponds to a hurricane of Saffir-Simpson Category 3, leading to the adoption of the term ‘winter hurricane’ to describe this class of very intense ETCs (e.g. Von Ahn *et al.*, 2006).

A new continuous 33-year global wave hindcast (GROW2012) based on a new atmospheric reanalysis wind field product provides unbiased estimates of the probability of exceedance of extratropical storm sea states with peak VESS threshold HS and small basin dependent biases (0.5–1.5 m) of peak HS greater than ~16 m. GROW2012, therefore, is a suitable database to be applied to a simulation to assess the risk of a merchant vessel that does not avail itself of weather routing guidance from government or private sources of encountering VESS sea states for typical NH and SH routes. Such a simulation was carried out for nine trade routes and for simulated departures in any month. The monthly exceedance probability (MEP) distributions resulting from these simulations suggest that at the HS threshold of 5–8 m, the SIO route simulated is harshest. However, at the VESS threshold of 14 m, the highest MEPs are in the NATL and NPAC at ~0.1% during winter months.

Analysis of an alternative statistical distribution of the monthly exceedance probability of the single maximum peak sea state to be expected for a voyage for any month (MEPm) revealed that the highest MEPm is for the month of December in the NAO along DB-BR route and in the NPO along YK-SE route at about 3%. In no month and for no route in the SO does MEPm exceed ~1.5% and this is for CP-ML in the July. We are left with the impression that while the SO are more likely to present sea states that present operational challenges, a vessel is more apt to encounter dangerous sea states along mid and high latitude NH routes.

The 33-year simulation based on 6-h daily departures also yields the duration of encounter along the simulated routes of extreme sea states of such magnitude, that is HS close to 20 m, that rogue waves of catastrophic heights of the order of say 40 m might also be encountered. On the basis of the actual mean voyage durations and assuming instant port turnaround, the mean number of hours of exposure to a vessel along each route during its 33-entire lifetime was estimated and was found to be typically less than ~3 h for six of the nine routes and a maximum of 10.2 h for two of the routes.

While along all routes simulated the results imply extremely small probabilities that a vessel will encounter the most VESS during its lifetime, the consequences of doing so in terms of cargo or vessel damage or loss are so catastrophic that the risk should be lowered by use of weather guidance. Such guidance is utilized typically in both a strategic sense for route planning, and tactical sense for on-route course adjustments to avoid ‘heavy weather’. The World Meteorological Organization (WMO) has coordinated well the efforts of the major international weather forecasting centers to ensure that there are ample marine forecast products available on a global basis to the maritime community to aid these efforts. Uncertainties in such forecast products may be addressed by utilizing ensembles of weather model forecasts. In addition, during the past decade there has emerged proprietary PC-based on-board weather routing systems to further aid voyage planning. The success of weather guidance, whether from public or proprietary sources, stems basically from the great strides made in the past few decades in the ability of modern numerical weather prediction models (NWP) operated at the major NWP centers, to foreshadow the tracks and intensity at horizons out to at least 5 days, of the class of ETCs that typically generate VESS, namely ‘winter hurricanes’, and the ability of advanced third-generation wave models to propagate that skill into reliable sea state predictions.

References

Ash E, Carter D, Collard F. 2011. *DUE GlobWave Wave Data Handbook*. Logica, UK Ltd., 58pp. http://www.globwave.org/content/download/10362/68974/file/GlobWave_D.9_WDH_v1.0.pdf

Bitner-Gregersen EM, Hagen O. 2004. Freak wave events within the second order wave model. In *Proceedings of 23rd International Conference on Offshore Mechanics and Arctic Engineering (OMAE)*. Vancouver, Canada.

Bitner-Gregersen EM, Toffoli A. 2012. On the probability of occurrence of rogue waves. *Nat. Hazards Earth Syst. Sci.* **12**: 751–762.

Brayshaw DJ, Hoskins B, Blackburn M. 2009. The basic ingredients of the North Atlantic storm track. Part 1: land-sea contrast and orography. *J. Atmos. Sci.* **66**: 2539–2559.

Buchner B, Forristall G, Ewans K, Christou M, Hennig J. 2011. New insights in extreme crest height distributions: a summary of the CREST JIP. OMAE 2011-49846, 19–24 June, Rotterdam, The Netherlands.

Cardone VJ, Jensen RE, Resio DT, Swail VR, Cox AT. 1996. Evaluation of contemporary ocean wave models in rare extreme events: Halloween storm of October, 1991; Storm of the century of March, 1993. *J. Atmos. Ocean. Technol.* **13**: 198–230.

Cardone VJ, Cox AT, Morrone MA, Swail VR. 2011. Global distribution and associated synoptic climatology of very extreme sea states (VESS). In *12th International Workshop on Wave Hindcasting and Coastal Hazards*. Hawaii, November 2012.

Carter DJT. 2011. Validation of high wave height data. GlobWave Misc Note.

Chao YY, Tolman H. 2010. Performance of NCEP regional wave models in predicting peak sea states during the 2005 North Atlantic hurricane season. *Weather Forecast.* **25**: 1543–1567.

Chelton DB, Ries JC, Haines BJ, Fu LL, Callahan PS. 2001. In *Satellite Altimetry and Earth Sciences*, Fu LL, Cazenave A (eds). Academic Press: San Diego, CA.

Chen H, Cardone VJ, Lacey P. 1998. Use of operation support information technology to increase ship safety and efficiency. In *Annual Meeting of Society of Naval Architects and Marine Engineers*. Vol. 106, 105–128.

Christou M, Ewans E. 2011. Examining a comprehensive dataset containing thousands of freak wave events. Part 2 – analysis and findings. OMAE2011-50169, 19–24 June, Rotterdam, The Netherlands.

Cox AT, Cardone VJ. 2011. On the use of the climate forecast system reanalysis wind forcing in ocean response modeling. In *12th International Workshop on Wave Hindcasting and Coastal Hazards*. Kona, Hawaii, October 31–November 4.

Cox AT, Swail VR. 2000. A global wave hindcast over the period 1958–1997: validation and climate assessment. *J. Geophy. Res. (Oceans)* **106**(C2): 2313–2329.

Cox AT, Wang X. 2013. Global wave climate trend and variability. In *13th International Workshop on Wave Hindcasting and Forecasting and 4th Coastal Hazards Symposium*. Banff, AB, Canada, October 27–November 1.

Faulkner D. 2001. An analytical assessment of the sinking of the M.V. Derbyshire. Transactions of the Royal Institution of Naval Architecture.

France W, Levadou M, Treakle TW, Pauling JR, Moore RK, Moore C. 2003. An investigation of head-sea parametric rolling and its influence on container lashing systems. *Marine Technol.* **40**(1): 1–19.

Garrett C, Gemmrich J. 2009. Rogue waves. Physics Today, American Institute of Physics, June, 2009.

Guedes Soares C, Cherneva Z, Antão EM. 2003. Characteristics of abnormal waves in North Sea storm sea states. *Appl. Ocean Res.* **25**: 337–344.

Guo B, Bitner-Gregersen E, Sun H, Bloch Helmers J. 2013. Prediction of ship based response statistics in extreme seas using model test data and numerical simulations based on the Rankline Panel Method. OMAE 2013, Nantes, France, 9–14 June, 2013.

Gyakum JR. 1983. On the evolution of the QE II storm. I: synoptic aspects. *Mon. Weather Rev.* **111**(6): 1137–1155.

Haver S, Andersen O. 2000. Freak waves: rare realizations of a typical population or typical realizations of a rare population. In *Proceedings of the 10th International Offshore and Polar Engineering Conference*. ISOPE, Seattle, USA, Vol. III, 123–130.

Holliday NP, Yelland MJ, Pascal R, Swail VR, Taylor PK, Griffiths CR, Kent E. 2006. Were extreme waves in the Rockall Trough the largest ever recorded? *Geophys. Res. Lett.* **33**: L05613, DOI: 10.1029/2005GL025238.

IACS. 2001. International Association of Classification Societies. Recommendation No. 34, Standard Wave Data. http://www.iacs.org.uk.

Jensen RE. Cardone VJ, Cox AT. 2006. Performance of third generation wave models in extreme hurricanes. In *9th International Wind and Wave Workshop*. Victoria, BC, Canada, 25–29 September.

Khandekar ML, Lalbeharry R, Cardone VJ. 1994. The performance of the Canadian spectral ocean wave model (CSOWM) during the Grand Banks ERS-1 SAR wave spectra validation experiment. *Atmosphere-Ocean* **32**: 31–60.

Lechuga A. 2006. Were freak waves involved in the sinking of the Tanker “Prestige”? *Nat. Hazards Earth Syst. Sci.* **6**: 973–978.

Magnusson AK, Donelan MA. 2012. The Andrea wave. Characteristics of a measured North Sea rogue wave. OMAE 2012-84099.

Monbaliu J, Toffoli A. 2003. Regional distribution of extreme waves. In *Proceedings of the MAXWAVE Final Meeting*. Geneva, Switzerland, 8–10 October.

Muir LR, El-Shaarawi AH. 1986. On the calculation of extreme wave heights: a review. *Ocean Eng.* **13**(1): 93–118.

Onorato M, Cavaleri L, Fouques S, Gramstad O, Janssen PAEM, Monbaliu J, Osborne AR, Pakozdi C, Serio M, Stansberg CT, Toffoli A, Trulsen K. 2009. Statistical properties of mechanically generated surface gravity waves: a laboratory experiment in a three dimensional wave basin. *J. Fluid Mech.* **626**: 235–257.

Pierson WJ, Moskowitz L. 1964. A proposed spectral form for fully developed wind seas based on the similarity theory of S. A. Kitaigorodskii. *J. Geophys. Res.* **69**: 5181–5190.

Queffeulou P, Croize-Fillon D. 2010. Global altimeter SWH data set. IFREMER, Plouzane France, May, 2010.

Rosenthal W, Lehner S. 2008. Rogue waves: results of the MaxWave Project. *J. Offshore Mech. Arct. Eng.* **130**(2): 8.

Saha S, Moorthi S, Pan H-L, Wu X, Wang J, Nadiga S, Tripp P, Kistler R, Woollen J, Behringer D, Liu H, Stokes D, Grumbine R, Gayno G, Wang J, Hou Y-T, Chuang H, Juang H-MH, Sela J, Iredell M, Treadon R, Kleist D, Van Delst P, Keyser D, Derber J, Ek M, Meng J, Wei H, Yang R, Lord S, van den Dool H, Kumar A, Wang W, Long C, Chelliah M, Xue Y, Huang B, Schemm J-K, Ebisuzaki W, Lin R, Xie P, Chen M, Zhou S, Higgins W, Zou C-Z, Liu Q, Chen Y, Han Y, Cucurull L, Reynolds RW, Rutledge G, Goldberg M. 2010. The NCEP climate forecast system reanalysis. *Bull. Am. Meteorol. Soc.* **91**: 1015–1057.

Sanders F, Gyakum JR. 1980. Synoptic-dynamic climatology of the “Bomb”. *Mon. Weather Rev.* **108**: 1589–1606.

Soares A, Swail VR. 2006. The WMO/IOC JCOMM Wave Programme. In *9th International Wind and Wave Workshop*. Victoria, BC, Canada, 25–29 September.

Socquet-Juglard H, Dysthe K, Trulesn K, Krogstad H, Liu J. 2005. Distribution of surface gravity waves during spectral changes. *J. Fluid Mech.* **542**: 195–216.

St Denis M, Pierson WJ. 1953. On the motions of ships in confused seas. Transactions of the Society of Naval Architecture and Marine Engineering.

Swail VR, Cox AT. 2000. On the use of NCEP/NCAR reanalysis surface marine wind fields for a long term north Atlantic wave Hindcast. *J. Atmos. Ocean. Technol.* **17**(4): 532–545.

Thibaut P, Ferreira F, Femenias P. 2007. Sigma0 blooms in the ENVISAT radar altimeter-dat. In *Proceedings of the ENVISAT Symposium 2007*. Montreux, Switzerland, 23–27 April 2007. ESA SP-636, July 2007.

Thompson EF, Cardone VJ. 1996. Practical modeling of hurricane surface wind fields. *J. Waterway, Port, Coastal, Ocean Eng.* **122**(4): 195–205.

Toffoli A, Lefevre JM, Bitner-Gregersen E, Monbaliu J. 2006. Towards the identification of warning criteria: analysis of a ship accident database. *Appl. Ocean Res.* **27**: 281–291.

Toffoli A, Gramstad O, Trulsen K, Monbaliu J, Bitner-gregersen E, Onorato M. 2010. Evolution of weakly nonlinear random directional waves: laboratory experiments and numerical Simulations. *J. Fluid Mech.* **664**: 313–336.

Von Ahn JM, Sienkiewicz JM, Chang P. 2006. Operational impact of QuikSCAT winds in the NOAA Ocean Prediction Center. *Weather Forecast.* **21**: 523–539.

Waseda T, Kinoshita T, Tamura H. 2009. Evolution of a random directional wave and freak wave occurrence. *J. Phys. Oceanograph.* **39**: 621–639.

